

See discussions, stats, and author profiles for this publication at: <https://www.researchgate.net/publication/272751247>

Enhancement of Organic Photovoltaic Efficiency via Nanomorphology Control using Conjugated Polymers Incorporating Fullerene Compatible Side-Chains

ARTICLE *in* MACROMOLECULES · JANUARY 2015

Impact Factor: 5.8 · DOI: 10.1021/ma502546b

CITATIONS

2

READS

48

14 AUTHORS, INCLUDING:



Hyunjung Kim

Sogang University

66 PUBLICATIONS 474 CITATIONS

[SEE PROFILE](#)



Doh-Kwon Lee

Korea Institute of Science and Technology

98 PUBLICATIONS 970 CITATIONS

[SEE PROFILE](#)



Jin Young Kim

Ulsan National Institute of Science and Techn...

496 PUBLICATIONS 9,021 CITATIONS

[SEE PROFILE](#)



Honggon Kim

Korea Institute of Science and Technology

87 PUBLICATIONS 941 CITATIONS

[SEE PROFILE](#)

Enhancement of Organic Photovoltaic Efficiency via Nanomorphology Control using Conjugated Polymers Incorporating Fullerene Compatible Side-Chains

Sungmin Park,^{†,‡,○} Dongkyun Seo,^{§,○} Tae In Ryu,^{||} Gukil Ahn,[⊥] Kyungwon Kwak,[§] Hyunjung Kim,[⊥] Cheol Hong Cheon,[‡] Nam-Gyu Park,^{||,#} BongSoo Kim,[†] Min Jae Ko,[†] Doh-Kwon Lee,[†] Jin Young Kim,[†] Honggon Kim,[†] and Hae Jung Son^{*,†}

[†] Photoelectronic Hybrid Research Center, Korea Institute of Science and Technology, Seoul 136-791, Korea

[‡] Department of Chemistry, Korea University, Seoul 136-713, Korea

[§] Department of Chemistry, Chung-Ang University, Seoul 156-756, Korea

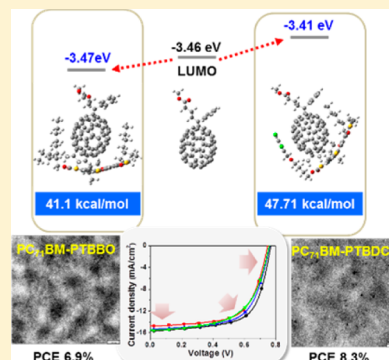
^{||} School of Chemical Engineering, Sungkyunkwan University, Suwon 440-746, Korea

[⊥] Department of Physics, Sogang University, Seoul 121-742, Korea

[#] Department of Energy Science, Sungkyunkwan University, Suwon 440-746, Korea

Supporting Information

ABSTRACT: We present controls of nanomorphology of polymer:fullerene BHJ films via synthesis of a series of push–pull-type copolymers with various molar percentages of side chains terminated with o-dichlorobenzyl (DCBZ) groups. As the molar percentage of the DCBZ-containing repeat units increases, the miscibility of the polymers in the series with PC₇₁BM increases with respect to that of the polymer (PTBBO) that does not contain DCBZ. In the optimal film morphology, which consists of a polymer containing 25 mol % DCBZ-terminated side chains in the electron-pull unit (PTBDCB25), the polymer/PC₇₁BM interface area is sufficiently large for efficient charge separation and percolated pathways is present for efficient charge carrier transport. In contrast, the BHJ film prepared from PTBBO has smaller interfaces and larger PC₇₁BM aggregates. Furthermore, the intermolecular interaction between PC₇₁BM and DCBZ induced changes in the PC₇₁BM's electronic structure at the polymer:PC₇₁BM interface, resulting in an increase of the PC₇₁BM's LUMO level and thereby the improved open-circuit voltage. As a result, the BHJ solar cell device fabricated with PTBDCB25 exhibits significantly improved performance with a PCE of 8.30%, whereas the PCE of PTBBO is 6.90%.



INTRODUCTION

Nanomorphology controls of polymer:fullerene bulk heterojunction (BHJ) films are of great importance for achieving high solar cell efficiencies in BHJ organic photovoltaics (OPVs) devices.^{1–8} To maximize free charge carrier generation and collection, the polymer and fullerene materials should develop a nanostructure such that their interface area is maximized, while typical dimensions of phase separation are within the exciton diffusion range (~ 10 nm) and continuous pathways for charge carrier transport to the electrodes are ensured.^{7,9–12} Additionally, it is required to form optimal polymer:fullerene nanostructures of the blend film in such a way to maximize open-circuit voltages (V_{oc}) because variations in the film morphology can modulate the device V_{oc} .^{13–15} To achieve high solar cell efficiencies, a thorough understanding of the relationship between the molecular structures of the polymer and the BHJ nanomorphology and the solar cell properties is necessary. In particular, it is important to identify a

correspondence between polymer–fullerene interactions and photovoltaic properties at a molecular level.^{16,17}

One of challenging tasks in the morphology control is to design conjugated polymers with good compatibility with fullerene derivatives. Most attempts to improve the miscibility of the polymer with the fullerene derivatives have been limited to tuning the properties of the polymer through modifying alkyl side chains such as the alkyl chain length and the bridging point.^{18–24} In some cases, fullerene molecules were found to intercalate between the neighbored polymer side chains and formed well intermixed morphology.^{25,26} Morphology control at a nanoscale was performed by introducing various polymer end-cappers, which effectively change the surface energy of the polymer and thus the miscibility with fullerenes.²⁷

Received: December 17, 2014

Revised: December 28, 2014

Published: January 15, 2015

The miscibility of the molecules can be characterized in terms of the Hansen solubility parameters (δ) of the blend components; materials with similar values of δ are likely to be mutually miscible via intermolecular interactions.^{28–31} Therefore, to increase the miscibility of the polymer with fullerenes, it would be beneficial to introduce functional moieties with Hansen solubility parameters close to those of fullerene derivatives as side chains, such as the o-dichlorobenzyl group (DCBZ).²⁸ o-Dichlorobenzene (ODCB) is a good solvent for fullerene derivatives as well as conjugated polymers and has been used as a representative solvent for processing polymer BHJ films. In addition, dipole moments generated on the ODCB side chain terminal are expected to play favorably for better molecular packing of the polymer and thereby better charge carrier transport.

Herein, we investigated morphological properties of polymer:fullerene BHJ films of push–pull-type random copolymers containing the DCBZ group at the ends of their alkyl side chains. In our study, we chose poly(thienothiophene-co-benzodithiophene) as the basic polymer backbone because it is a good low bandgap polymer for the BHJ solar cells.^{32,33} Tuning the molar portion of the DCBZ functionalized side chain in the polymer effectively controlled the miscibility of the polymer and PC₇₁BM and thus optimized the nanoscale phase separation in the polymer:PC₇₁BM BHJ active layer, resulting in the improved short-circuit current (J_{sc}). Moreover, the introduced DCBZ group was demonstrated to induce changes in the PC₇₁BM's electronic structure, which resulted in the increased lowest unoccupied molecular orbital (LUMO) energy level of PC₇₁BM at the interface of polymer/PC₇₁BM and thereby the enhanced V_{oc} of polymer BHJ solar cells. As a result, DCBZ-based polymer solar cells achieved a high power conversion efficiency (PCE) up to 8.30%.

RESULTS AND DISCUSSION

We introduced the DCBZ group into the polymers via random copolymerization of 2-butyloctyl 4,6-dibromo-3-fluorothieno[3,4-*b*]thiophene-2-carboxylate (TT-BO), 4-(3,4-dichlorobenzyl)butyl 4,6-dibromo-3-fluorothieno[3,4-*b*]thiophene-2-carboxylate (TT-DCBZ), and 2,6-bis(trimethyltin)-4,8-bis(2-ethylhexyloxy)benzo[1,2-*b*:4,5-*b'*]dithiophene (BDT-EH). These monomers were synthesized by following modified literature procedures^{21,34} and the polymerization was carried out via the Stille coupling polymerization³⁵ with the prepared monomers at feed ratios of TT-BO:TT-DCBZ=m:n (mol:mol) = 1:0, 0.75:0.25, 0.5:0.5, and 0:1 to produce PTBBO, PTBDCB25, PTBDCB50, and PTBDCB100, respectively (Figure 1a). The polymerized products were precipitated in methanol, and purified by performing successive Soxhlet extractions with methanol, hexane, and chloroform. The molecular weights of PTBBO, PTBDCB25, PTBDCB50, and PTBDCB100 were estimated with gel permeation chromatography (GPC) at 80 °C and found to be M_n = 69, 70, 65, and 51 kg/mol with polydispersity indices (PDI) of 2.8, 2.5, 2.3, and 2.5, respectively.

The UV–vis absorption spectra of the polymers in a film are shown in Figure 1b and their characteristic data are summarized in Table 1. The absorption spectrum is slightly red-shifted as the proportion of TT-DCBZ in the polymer increases and thus the onset point (λ_{onset}) and maximum peak (λ_{max}) are red-shifted by ~10 nm from PTBBO (λ_{onset} = 745 nm, λ_{max} = 675 nm) to PTBDCB100 (λ_{onset} = 756 nm, λ_{max} = 683 nm). The optical energy bandgaps (E_g^{opt}) of PTBBO, PTBDCB25, and

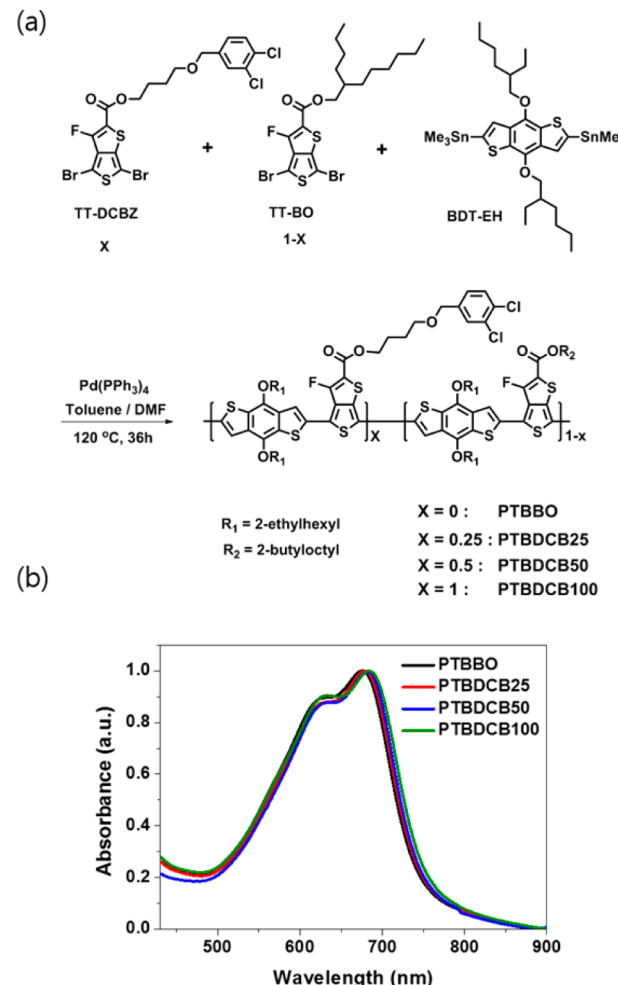


Figure 1. (a) Synthesis of PTBBO, PTBDCB25, PTBDCB50, and PTBDCB100. (b) UV–vis absorption spectra of the polymers in a film casted from chlorobenzene solutions.

Table 1. Optical and Electrochemical Properties of the Polymers

polymer	λ_{max} (nm)	λ_{onset} (nm)	E_g^{opt} (eV)	IP (eV)	EA (eV)
PTBBO	675	745	1.66	5.17	3.34
PTBDCB25	678	746	1.66	5.10	3.22
PTBDCB50	681	749	1.66	5.05	3.25
PTBDCB100	683	756	1.64	4.95	3.27

PTBDCB50 are estimated to be ~1.66 eV from the onset points of the absorption spectra and PTBDCB100 shows a decreased E_g value of 1.64 eV. The electrochemical properties of the polymers were investigated by using cyclic voltammetry (CV) (Figure S1, Supporting Information). The electron affinity (EA) and the ionization potential (IP) energies of the polymers were determined from the onset of the reduction and oxidation potentials, respectively as shown in Table 1.^{33,36} Both of the IP and EA energies of the polymers were shifted up as the molar ratio of the TT-DCBZ in the polymer backbone increased and thus, the IP energy of PTBDCB100 (4.95 eV) was 0.22 eV lower than 5.17 eV of PTBBO. Incorporation of the DCBZ group would induce conformational changes of the polymer backbone, which resulted in the red-shifted UV–vis absorption spectra and the change in electrochemical properties.

We fabricated solar cells utilizing the prepared polymers in active layers composed of polymer:PC₇₁BM blends. The solar cell device structure is indium tin oxide (ITO)/poly(3,4-ethylenedioxythiophene):poly(styrenesulfonate) (PEDOT:PSS)/polymer:PC₇₁BM (1:1.5 wt/wt)/TiO₂/Al. The current–voltage (J – V) curves of the polymer solar cell devices are shown in Figure 2a and the best and average values of their characteristic photovoltaic parameters are given in Table 2. Overall, the polymers containing DCBZ exhibit better solar cell performances than PTBBO due to their improved J_{sc} values. In the histograms of statistical J_{sc} values (Figure 2d), the DCBZ-based polymer showed ~1 mA/cm² higher values. In the external quantum efficiency (EQE) spectra of the polymer solar cells (Figure 2b), the EQE values for the range 450–800 nm of all the polymers containing DCBZ are higher than that of PTBBO. The onset point of the PTBDCB100 EQE spectrum is slightly red-shifted with respect to those of the other polymers due to its lower energy bandgap. The highest PCE of 7.87% was obtained for the PTBDCB25 device with an open-circuit voltage (V_{oc}) of 0.77 V, a fill factor (FF) of 0.651, and a J_{sc} of 15.70 mA/cm² (Table 2). However, when the DCBZ content of the polymer is increased above that of PTBDCB25, the solar cell efficiency gradually decreases, which is mainly due to decreases in FF. As a result, PTBDCB100 showed the lowest PCE of 6.96% among the DCBZ based polymers with a FF of 0.589. The V_{oc} values of the polymer devices are in the range 0.76–0.77 V and notably, higher than 0.74 V of PTBBO despite that the IP energies of the DCBZ based polymers (4.95–5.10 eV) are 0.07–0.22 eV lower compared with PTBBO (5.17 eV). Furthermore, the V_{oc} of PTBDCB100 (0.76 V) is a significantly improved value compared with PTB1 (0.58 V) and PTB2 (0.60 V) polymers in spite of their similar polymer structures and IP energies (4.8 eV for PTB1, 4.94 eV for PTB2, and 4.95 for PTBDCB100) to each other.²¹ Regarding this, we will discuss further in the next “theoretical study” section. By tuning the weight ratio of the polymer:PC₇₁BM composite from 1:1.5 to 1:1, the solar cell efficiency of PTBDCB25 was further improved up to 8.30% with a J_{sc} of 16.22 mA/cm², a V_{oc} of 0.76 V, and a FF of 0.673 (Figure 2c).

To investigate the influence of the DCBZ functionalization of the polymer on the polymer solar cell properties, we investigated the nanostructural properties of the polymer:PC₇₁BM BHJ films in the solar cell devices with transmission electron microscopy (TEM). Figure 3 shows the TEM images of the BHJ blend films. It is found that the size and density of dark regions due to PC₇₁BM aggregation decreases as the TT-DCBZ content in the polymer increases. The PTBBO blend film contains 100–200 nm PC₇₁BM-rich domains, whereas the PTBDCB25 and PTBDCB50 blend films have more uniformly intermixed morphologies with nanoscale percolating networks. PTBDCB100 has a homogeneous morphology with very fine features, which indicates that the miscibility of PTBDCB100 with PC₇₁BM is very high. The improved nanomorphology of the DCBZ incorporated polymer blend film is advantageous for enhancing charge carrier generation at the polymer/PC₇₁BM interface in the polymer BHJ solar cells and thereby improve J_{sc} s; the nanoscale phase separation will increase the probability that the exciton reaches the interface and is dissociated into charge carriers when considering the limited exciton diffusion lengths of conjugated polymers due to the short exciton life times.^{9,37} On the other hand, if the degree of intermolecular mixing between the

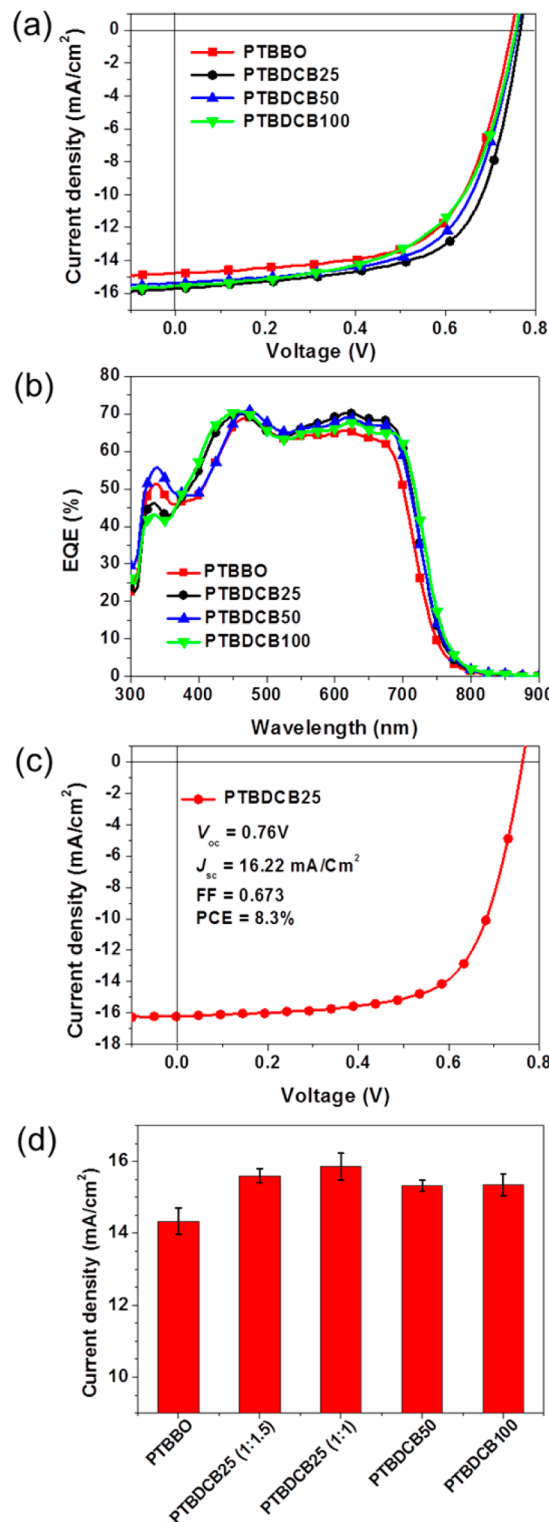


Figure 2. (a) J – V curves and (b) EQE spectra of the polymer:PC₇₁BM (1:1.5) solar cells. (c) J – V curve of the PTBDCB25:PC₇₁BM (1:1.1) solar cell. (d) Histogram of statistical J_{sc} values for the solar cells.

polymer and PC₇₁BM is too high such as in PTBDCB100, poor charge transport pathways and thus bimolecular recombination are likely to result. The decreased FF and lower EQEs of the PTBDCB100 solar cell in 500–800 nm are probably due to such morphology. We performed a TOF-SIMS to investigate the compositional gradient of each polymer:PC₇₁BM blend

Table 2. Characteristics of the Polymer Solar Cells

polymers	polymer:PC ₇₁ BM	V _{oc} (V)	J _{sc} (mA/cm ²)	FF	efficiency (max) (%)	efficiency (av) ^a (%)
PTBBO	1:1.5	0.74	14.76	0.632	6.90	(6.88 ± 0.13)
PTBDCB25	1:1.5	0.77	15.70	0.651	7.87	(7.70 ± 0.10)
	1:1.1	0.76	16.22	0.673	8.30	(8.0 ± 0.23)
PTBDCB50	1:1.3	0.76	15.39	0.640	7.49	(7.37 ± 0.11)
PTBDCB100	1:1.3	0.76	15.54	0.589	6.96	(6.90 ± 0.13)

^aAverage PCE of 18 devices fabricated under identical conditions.

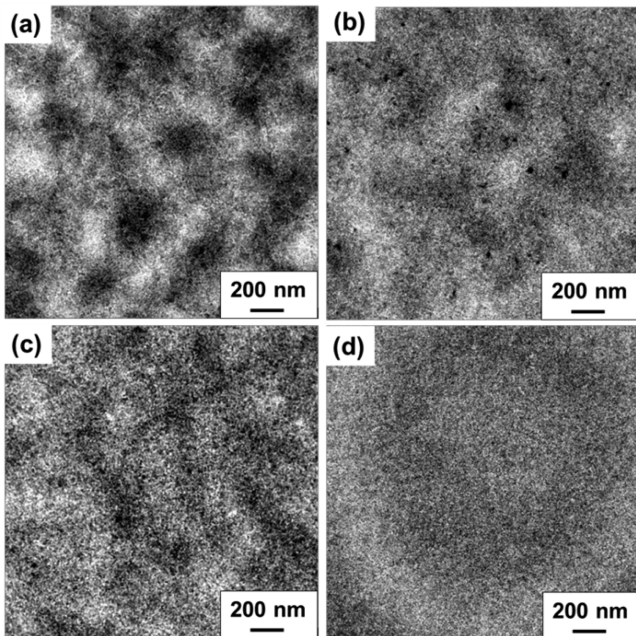


Figure 3. TEM images of the polymer:PC₇₁BM (1:1.5) blend films prepared from the polymers of (a) PTBBO, (b) PTBDCB25, (c) PTBDCB50, and (d) PTBDCB100.

layer. For identifying the polymers, the F⁻ ($m/q = 19$) and Cl⁻ ($m/q = 35.5$) signals were recorded and normalized to C₂⁻ signals ($m/q = 24$) as a function of depth. Depth profiles of the F⁻/C₂⁻ and Cl⁻/C₂⁻ signal ratios were obtained for active layers prepared using different polymers with a film structure of ITO/PEDOT:PSS/polymer:PC₇₁BM (Figure S2); For all blend films, in common, each Cl⁻/C₂⁻ and F⁻/C₂⁻ signal is constant throughout the active layer, suggesting that there is a homogeneous distribution of the polymer phases in the vertical direction.

To obtain a deeper understanding of the nanomorphologies of the polymer:PC₇₁BM blend films at a molecular level, grazing incidence X-ray diffraction (GIXD) patterns were recorded for the pristine polymers and the blend films. Figure 4 shows these GIXD patterns and the q_z line cut profiles. The patterns for the pristine films of the polymers all contain (010) diffraction peaks along the q_z direction at 1.62–1.64 Å⁻¹, which indicates that their π–π stacking distances are similar in the range 3.83–3.87 Å and that the polymer chains mainly remain in the face-on conformation after the introduction of the DCBZ group. In in-plane profiles of the pristine polymer (Figure S3), the (100) peaks of PTBDCB50 (0.30 Å⁻¹) and PTBDCB100 (0.31 Å⁻¹) are positioned at higher values than PTBBO (0.28 Å⁻¹) and PTBDCB25 (0.28 Å⁻¹), showing the lamellar stacking distances of PTBDCB50 (20.9 Å) and PTBDCB100 (20.3 Å) are shorter than PTBBO (22.4 Å) and PTBDCB25 (22.4 Å).

This is because PTBBO and PTBDCB25 contain relatively large portions of the long 2-butyl octyl group when compared with the other polymers. The π–π stacking peaks of PTBDCB50 and PTBDCB100 are more intensive than those of PTBBO and PTBDCB25 although the peaks corresponding to the lamellar spacing are similar in their intensities. This suggests that introduction of the DCBZ group is favorable for effective π–π stacking of the polymer chain. After blending with PC₇₁BM, the lamellar distances of all polymers were slightly decreased by about 2 Å (Figure S4), and the resulting distances are summarized in Table S1. The GIXD patterns for the polymer:PC₇₁BM blend films contain a scattering peak at $q_z = \sim 1.34$ Å⁻¹, which is due to the Bragg diffraction of PC₇₁BM.³⁸ As shown in the out of plane GIXD profile of the polymer:PC₇₁BM blend film, the incorporation of the DCBZ group into the polymer results in a weaker scattering peak of PC₇₁BM than that of PTBBO. Full widths at half-maximum (fwhm) of scattering peaks correlated to nanocrystallite sizes via the Scherrer equation ($DL = 2(\ln 2/\pi)^{1/2}2\pi(\Delta q)^{-1}$, where Δq is the intrinsic fwhm of the peak).³⁹ In the in-plane GIXD profile (Figure S5), Gaussian fits were used to determine peak FWHMs, as represented using black solid lines for the peak profiles. The measured Δq values are 0.266, 0.293, 0.296, and 0.274 Å⁻¹ for PTBBO, PTBDCB25, PTBDCB50, and PTBDCB100, respectively. Thus, the calculated PC₇₁BM crystallite sizes in the blend films are estimated to be 22.17, 20.13, 19.92, and 21.52 Å, for PTBBO, PTBDCB25, PTBDCB50, and PTBDCB100, respectively. This result implies that the crystallinity and sizes of the PC₇₁BM nanocrystallites were reduced after incorporation of the DCBZ unit. The high crystallinity of PC₇₁BM in the PTBBO:PC₇₁BM film would correlate with the high level of PC₇₁BM aggregation evident in the TEM image of the PTBBO:PC₇₁BM film. In general, conjugated polymers with high π–π stacking properties exhibit lower miscibility with fullerene derivatives because their self-organization properties disturb intermixing with other compounds and thus lead to large scale phase segregation.^{40,41} The nanoscale phase separation of the PTBDCB50 and PTBDCB100 blend films is much improved although PTBDCB50 and PTBDCB100 show more effective π–π stacking structures than that of PTBBO. This is probably due to the enhanced intermolecular interactions between the DCBZ group and PC₇₁BM such as the chlorine–fullerene or dipole–π interactions,^{42,43} which result in better compatibility between the polymers and PC₇₁BM and thereby in the well intermixed polymer:PC₇₁BM blend films. Taken together, the TEM and GIXD results show that the introduction of DCBZ groups into the polymers dissolves aggregated PC₇₁BM clusters in the polymer:PC₇₁BM blend films by making the polymer chains more miscible with PC₇₁BM.

We compared the surface energies of the polymers calculated using Owens–Wendt geometric mean equation. It is reported that when the surface energy values of the individual

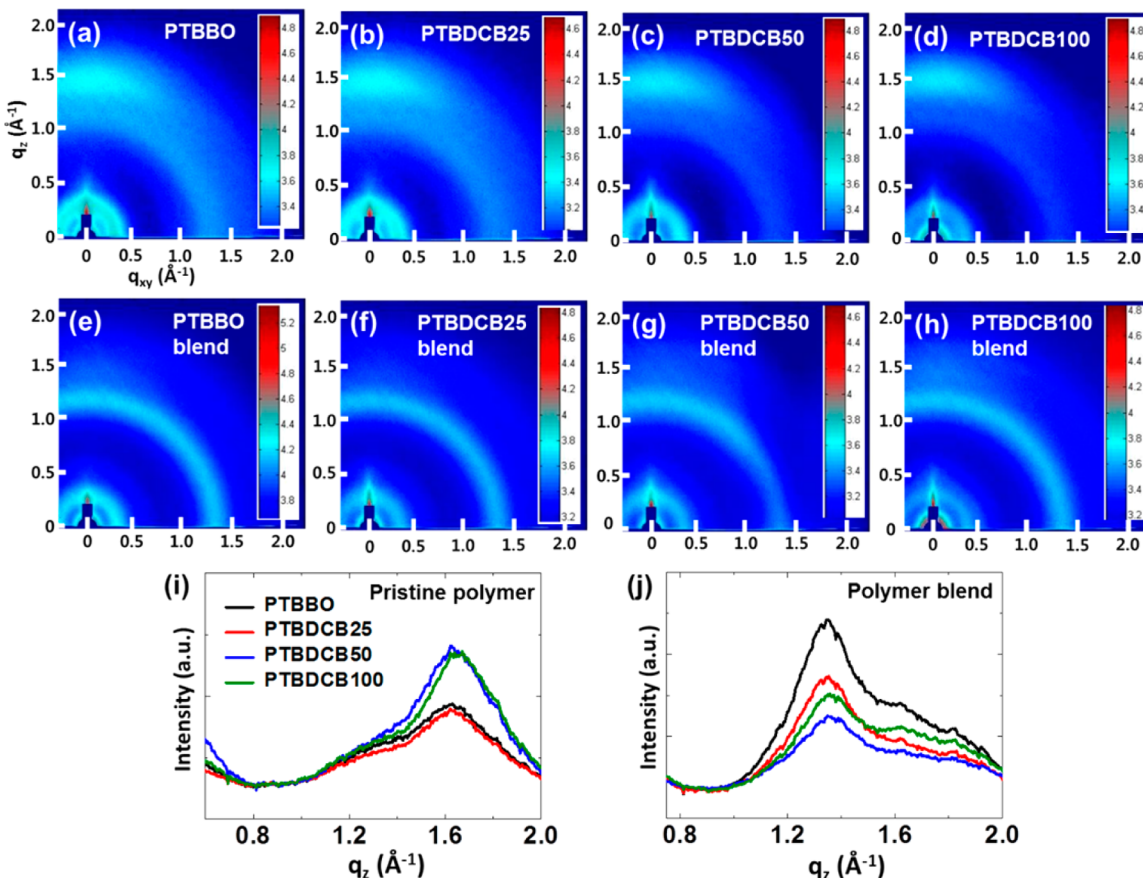


Figure 4. GIXD images of the polymer films of (a) PTBBO, (b) PTBDCB25, (c) PTBDCB50, and (d) PTBDCB100 and the polymer:PC₇₁BM (1:1.5) blend films of (e) PTBBO, (f) PTBDCB25, (g) PTBDCB50, and (h) PTBDCB100. Out-of-plane X-ray profiles of (i) the pristine polymer films and (j) the polymer:PC₇₁BM (1:1.5) blend films.

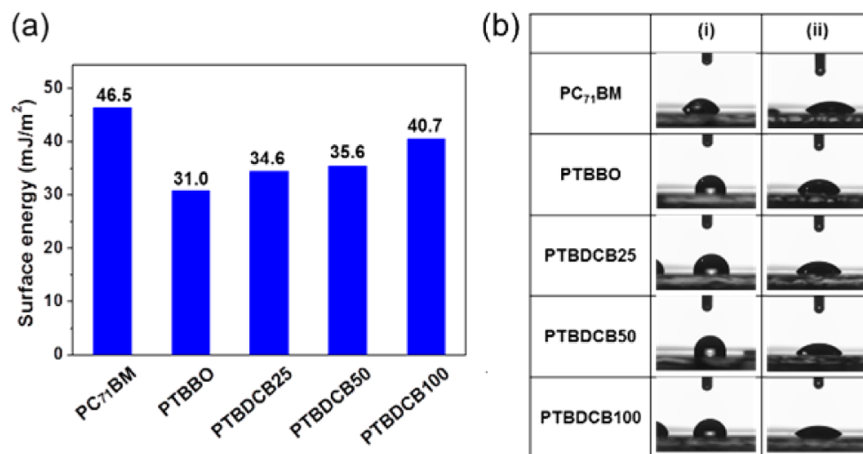


Figure 5. (a) Comparison of surface energy values of the polymers. (b) (i) H₂O and (ii) diiodomethane drops on the PC₇₁BM and polymer surfaces showing contact angles.

components of the blend films are similar, they exhibit better miscibility, which leads to more homogeneously mixed film morphologies.^{16,44} Figure 5 and Table S2 summarize the contact angle and surface energy values of the polymers. The polymer with the highest proportion of DCBZ has the largest surface energy close to that of PC₇₁BM: the surface energy of PTBDCB100 (40.7 mJ/m²) is more similar to 46.5 mJ/m² of PC₇₁BM compared to 31.0 mJ/m² of PTBBO. This is

correlated to the homogeneous and fine-featured morphology of the PTBDCB100:PC₇₁BM blend films.

Density function theory (DFT) calculations were performed to reveal the molecular details of the increased molecular interactions between the DCBZ-based polymer and PC₇₁BM, which may result in the improved solar cell properties of the DCBZ-incorporated polymers. The ground state geometries of the PC₇₁BM-polymer complexes and their respective isolated molecules have been fully optimized using Gaussian 09

software package. We used B3LYP correlation functional with a 6-311G (d,p) standard basis set on all atoms in a gas phase. Although DFT with B3LYP functional has been commonly used, it has been proved that this method could not properly describe dispersive interactions. Therefore, we employed D3 version of Gremme's dispersion with Becke-Johnson damping (GD3BJ) to investigate the intermolecular interaction of PC₇₁BM-polymer complexes adequately.⁴⁵ The configurations of the energy optimized structures of PC₇₁BM-monomer and PC₇₁BM-side chain complexes are shown in Figure 6. The

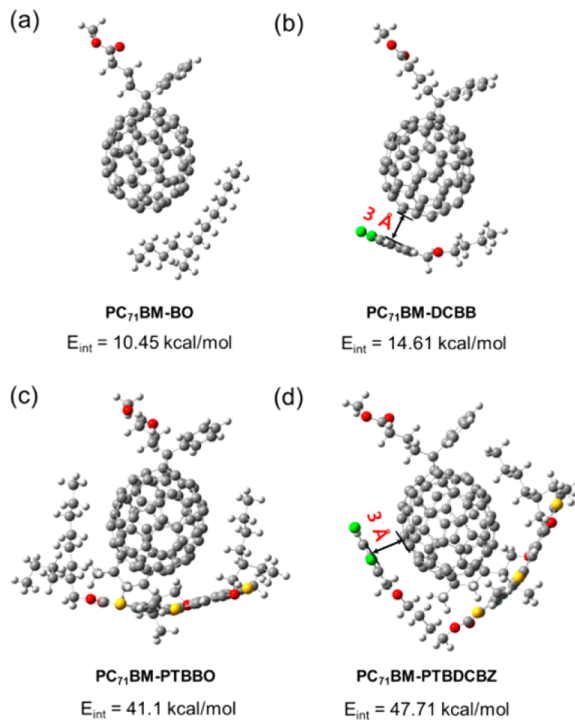


Figure 6. Optimized structures of PC₇₁BM-BO, PC₇₁BM-DCBB, PC₇₁BM-PTBBO, and PC₇₁BM-PTBDCBZ complexes and interaction energies (E_{int}) of BO, DCBB or PTBBO, PTBDCBZ with PC₇₁BM.

interaction energy of PC₇₁BM with 3,4-dichlorobenzylxybutane (DCBB) (14.61 kcal/mol, Figure 6b) is larger than that with 2-butyloctane (BO) (10.45 kcal/mol, Figure 6a). Interestingly, the enhancement value of 4.16 kcal/mol is comparable to the increase of the interaction energy from 41.1 to 47.71 kcal/mol in the PC₇₁BM-monomer complex system when a 2-butyl octyl side chain in the monomer is replaced by a 3,4-dichlorobenzylxybutyl group in Figure 6c,d. The stabilization energy values of the PC₇₁BM-DCBB complex were calculated with varying the distance between PC₇₁BM and DCBB and recorded in Figure S6. The distance yielding the highest stabilization energy (3 Å) is identical to that between the PC₇₁BM and DCBZ group in the PC₇₁BM-PTBDCBZ complex (Figure 6d).

This result indicates that the incorporation of the DCBZ into the polymer makes PC₇₁BM–polymer interactions energetically favorable and thus increases the miscibility of the polymer with PC₇₁BM. Moreover, the DCBZ group may act to hold the PC₇₁BM molecules so as to prevent large scale phase segregations when polymer:PC₇₁BM blends form BHJ films in polymer solar cell devices. Frontier orbital diagrams of the PC₇₁BM-monomer complexes are shown in Figure 7a. For both monomers, the HOMO of the complex is

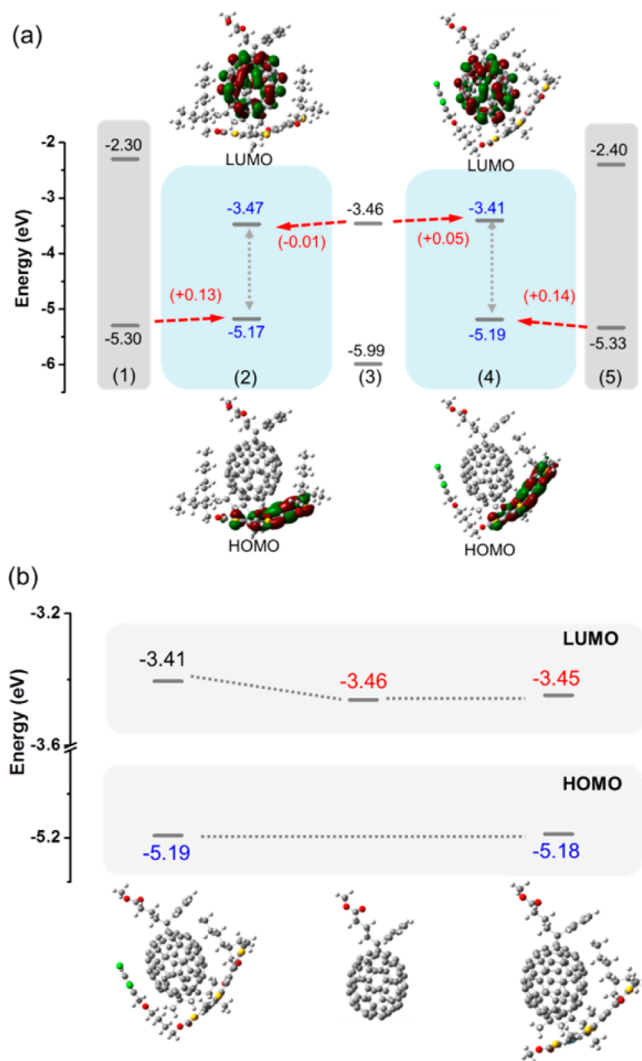


Figure 7. (a) Calculated HOMO and LUMO energy levels of (1) PTBBO, (2) PC₇₁BM-PTBBO, (3) PC₇₁BM, (4) PC₇₁BM-PTBDCBZ, and (5) PTBDCBZ. (b) Comparison of HOMO and LUMO energy levels of PC₇₁BM-PTBDCBZ, PC₇₁BM, and PC₇₁BM-PTBDCBZ without the DCBZ group.

essentially confined on the monomer donor while the LUMO is on the PC₇₁BM acceptor. The HOMO energy levels of the PC₇₁BM-PTBDCBZ and PC₇₁BM-PTBBO complexes are, in common, shifted up by 0.13–0.14 eV from the HOMO levels of their respective isolated monomer molecules. Interestingly, compared with the computed LUMOs of PC₇₁BM, the LUMO of PC₇₁BM-PTBDCBZ is increased by about 0.05 eV while that of PC₇₁BM-PTBBO is decreased by about 0.01 eV. As a result, the energy bandgap of PC₇₁BM-PTBDCBZ is 0.08 eV larger than that of PC₇₁BM-PTBBO. This is consistent with the observation of the larger V_{oc} values for the DCBZ incorporated polymers (0.76–0.77 V) than for PTBBO (0.74 V) despite that the former polymers have 0.07–0.22 eV lower IP energy levels, as determined by the CV experiment. For a deeper understanding of the effects of the intermolecular interaction between the DCBZ group in the polymer and PC₇₁BM on the energy levels of the complex, we detached the DCBZ group from the complex and observed the resulting energy levels (Figure 7b); the LUMO energy level was lowered to -3.45 eV and became similar to that of the isolated PC₇₁BM (-3.46 eV)

while the HOMO level (-5.18 eV) remained close to that of PC₇₁BM-PTBDCBZ (-5.19 eV), suggesting that the DCBZ group in the polymer predominantly influenced the LUMO energy level of the PC₇₁BM–polymer complex. In addition, we investigated how the LUMO energy level of PC₇₁BM is affected by the interactions with DCBB because the LUMO of the PC₇₁BM-PTBDCBZ complex is mostly localized on PC₇₁BM and reflected by PC₇₁BM's LUMO. As shown in Figure S7, on forming a PC₇₁BM-DCBZ complex, the LUMO level of PC₇₁BM is increased to -3.41 eV, which is identical to the LUMO level of the PC₇₁BM-PTBDCBZ complex. By contrast, the LUMO level of PC₇₁BM is shifted down when the polymer interacts with BO, in agreement with the result obtained for the PC₇₁BM-PTBBO complex. As shown in Figure S8, changing the distance between PC₇₁BM and DCBB resulted in different frontier orbital energy levels of PC₇₁BM. In particular, the LUMO level at 3 \AA , which was found to be the optimal distance for the effective interaction between PC₇₁BM and DCBZ, is identical to that of the PC₇₁BM-PTBDCBZ complex. From the computational results, it is expected that the DCBZ in the polymer induced the increase of the LUMO level of PC₇₁BM positioned at the PC₇₁BM/polymer interface of the BHJ solar cell devices by the intermolecular interactions between the PC₇₁BM and the DCBZ group, resulting in the V_{oc} enhancement of the DCBZ-based polymer solar cells. It is observed that the geometry of the PC₇₁BM detached from the PC₇₁BM-PTBDCBZ (PC₇₁BM cpx) complex differs from that of the original structure (PC₇₁BM org) (Figure S9), leading to a decrease in the dipole moment from 4.59 D for PC₇₁BM org to 4.55 D for PC₇₁BM cpx. The computed total energy of PC₇₁BM is increased by about 0.48 kcal/mol after the deformation. It is expected that the intermolecular interaction between PC₇₁BM and the DCBZ group in the complex led to the changes in both the geometry and the electronic structure of PC₇₁BM, resulting in the increase in the LUMO energy level.

To further clarify the effects of the morphological changes on the photovoltaic properties, we performed a series of experiments as follows. First, we assessed the charge carrier mobilities of the devices; a high charge carrier mobility reduces bimolecular charge recombination after free charge carrier generation.^{46,47} The hole mobilities of the polymer: PC₇₁BM BHJ films were measured by using the space charge limited current (SCLC) method (Figure S10). The mobilities of the blend films were found to be 1.6×10^{-4} , 1.3×10^{-4} , 9.8×10^{-5} , and 7.0×10^{-5} cm² V⁻¹ s⁻¹ for PTBBO, PTBDCB25, PTBDCB50, and PTBDCB100, respectively; as more DCBZ is incorporated into the polymer, the mobility in its blend film gradually decreases. This gradual decrease probably arises because charge transport is more disturbed by the limited transport pathway as the polymer is more miscible with PC₇₁BM. This hypothesis is supported by the observation that the mobility in the PTBDCB100 blend film is the lowest among the polymer blend films despite its high $\pi-\pi$ stacking property in the GIXD result of the pristine polymer film. The lower FF value of the PTBDCB100 device compared with those of the other devices is related with the decreased charge transport of PTBDCB100, which may lead to the increase of bimolecular recombination in the solar cell device. Thus, the higher photocurrent levels of the DCBZ-based polymer devices cannot be explained in terms of charge transport and other factors need to be explored.

Next, the efficiency of charge carrier generation at the polymer/PC₇₁BM interfaces should be considered. From the

calculated energy offsets between the LUMO energy levels of the polymer and PC₇₁BM (~ -3.7 eV),²¹ each polymer solar cell is expected to have sufficient driving force to produce efficient charge transfer/separation at its polymer/PC₇₁BM interface. In fact, the photon energy losses of the polymer devices, which are defined by $E_g - eV_{oc}$, are similar, with values of 0.92 , 0.89 , 0.90 , and 0.88 eV for PTBBO, PTBDCB25, PTBDCB50, and PTBDCB100, respectively. These results suggest that the polymers have similar quantum efficiencies of charge generation.⁴⁸

Third, photocurrent generation is usually explained in terms of nongeminate recombination. We determined the dependence on light intensity of the photocurrent density for each of the PTBBO and PTBDCB25 solar cell devices, in order to characterize their recombination mechanisms. This dependence can be modeled with a power law relationship $J \propto P^\alpha$ where P is the power generation rate and the deviation of α from unity is due to bimolecular recombination and the buildup of space charges in the active layer.^{49–51} Figure S7 shows the photocurrent densities ($J_{ph} = J_L - J_D$) as functions of light intensity at the various effective voltages, where J_L and J_D are the current density under illumination and in the dark, respectively. The effective voltage is defined as $V_{eff} = V_0 - V_{appl}$ where V_0 is the compensation voltage at $J_{ph} = 0$ and V_{appl} is the applied voltage. For both of the polymer devices, there is a linear relationship between the logarithmic scales of the photocurrent density and the light intensity at V_{eff} values of 0.1 V, short-circuit, and 1.5 V, respectively, and at the given V_{eff} , the slopes of the polymers are very similar to each other; the slopes are ~ 0.91 at the short-circuit condition and $V_{eff} = 1.5$ V, and 0.81 – 0.82 at $V_{eff} = 0.1$ V. The result indicates that the degrees of bimolecular recombination and space charge effects are similarly small for both of the polymer solar cells.^{50,51}

Finally, the enlarged interface area in the polymer:PC₇₁BM blend films with the introduction of DCBZ into the polymers might result in increases of the probabilities that the photogenerated excitons reach the polymer:PC₇₁BM interfaces and separate into free charge carriers. To verify this hypothesis, we examined the photoluminescence (PL) quenching of polymer:PC₇₁BM blend films prepared under the same conditions as the solar cell active layers. Parts a and b of Figure 8 show the PL spectra recorded with excitations at 380 and 675 nm, respectively, and the maximum PL peaks of PC₇₁BM and the polymers are at 700 and 750 nm, respectively. In the pristine polymer films, all polymers showed almost identical PL spectra to each other. It is found that the PL quenching degree at both 700 and 750 nm is correlated with the DCBZ content of the polymer; the polymers with a higher DCBZ proportion exhibit a higher degree of PL quenching. In particular, because the PL from excitation at 380 nm is PC₇₁BM emission dominant,^{6,52} the degree of PL quenching after 380 nm excitation is able to stay relative to nonradiative quenching of excitons within the PC₇₁BM nanoclusters by the polymer. Two mechanisms possibly contributed to the quenching of PC₇₁BM emission in the blend film: hole transfer to the polymer or resonant energy transfer (RET) to the polymer. The PL spectrum of PC₇₁BM is well overlapped with the absorption spectra of the polymers in the range of 670 – 800 nm. Both of the quenching processes are dependent on the distance from the exciton to the polymer chain present near the polymer:PC₇₁BM interface.^{53–55} Therefore, from the relative PL intensity for the 380 nm excitation, we can estimate the relative sizes of the PC₇₁BM nanoclusters and the total

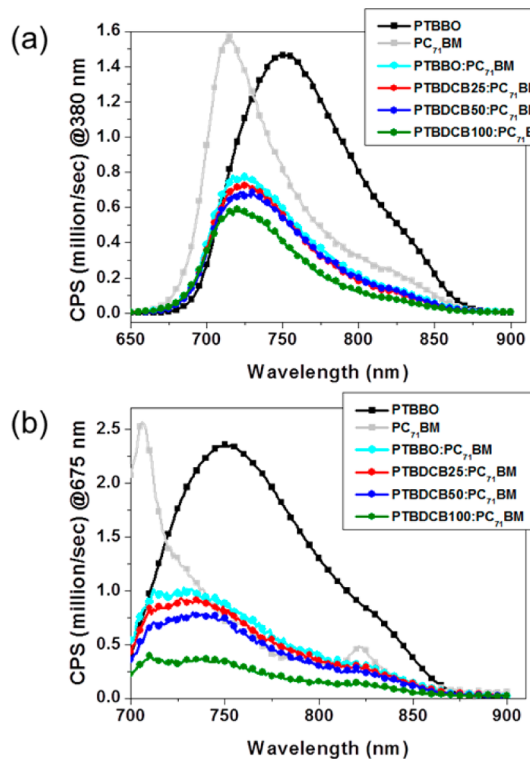


Figure 8. PL spectra of the polymer, PC₇₁BM and the polymer:PC₇₁BM blends with photoexcitation at (a) 380 nm and (b) 675 nm for PTBBO, PTBDCB25, PTBDCB50, and PTBDCB100: the PL spectra of the blend films are magnified with 10 and 40 times for parts a and b, respectively.

polymer/PC₇₁BM interface areas of the blend films: for the PC₇₁BM nanocluster sizes PTBBO > PTBDCB25 > PTBDCB50 > PTBDCB100 and for the interface areas PTBDCB100 > PTBDCB50 > PTBDCB25 > PTBBO. These results confirm that the incorporation of DCBZ at the terminal of the side chains makes the polymer chains more miscible with PC₇₁BM and thus increases the polymer:PC₇₁BM interface area, which results in more efficient charge carrier generation and thereby the J_{sc} enhancement in the solar cells.

As a result, the improvement in the photocurrent densities of the devices with the polymers containing DCBZ is mainly due to the improved exciton dissociation into free charge carriers. This is mostly contributed by the increased polymer/PC₇₁BM interface area resulting from the better miscibility of the polymers containing DCBZ with PC₇₁BM. However, excessive DCBZ incorporation resulted in decreases in FF (for the PTBDCB25 device, FF = 0.651, and for the PTBDCB100 device, FF = 0.589), which are due to the reduction in charge transport arising from limited pathways in the excessively intermixed BHJ film. Therefore, it is vital to optimize the morphology of the polymer:PC₇₁BM blend film with respect to phase separation by incorporating an proper amount of the DCBZ group into the polymer.

CONCLUSIONS

We have presented the control of the molecular interaction of polymer and PC₇₁BM via the synthesis of push–pull-type random copolymers containing various ratios of TT-DCBZ and TT-BO accepting units and their effects on photovoltaic properties. Introduction of the DCBZ group into the polymer resulted in several positive effects. First, the DCBZ group

enhanced the compatibility of the polymer with PC₇₁BM without having detrimental effects on the polymer's physical properties such as its optical properties or polymer packing structures in the solid state. Therefore, we can obtain optimal film morphology for achieving high solar cell efficiencies. More importantly, the interaction between PC₇₁BM and DCBZ induced the PC₇₁BM's molecular geometry to a higher energy state and changed the PC₇₁BM's electronic structure. This led to the increase of the PC₇₁BM's LUMO level and thereby the enhanced V_{oc} . Additionally, because of the versatility of this copolymerization-based approach, it can be readily extended to other conjugated polymeric systems for use in polymer:fullerene BHJ based solar cells. As a result, by tuning the ratio of TT-DCBZ and TT-BO monomers, the polymer solar cell employing PTBDCB25 was fabricated with a PCE of 8.30%. We believe that the random copolymerization of monomers with fullerene-compatible functional groups is an effective way for simultaneously enhancing J_{sc} and V_{oc} by controlling the nanomorphology and the electronic structure of acceptors in donor:acceptor BHJ solar cells. We are exploring other fullerene-compatible functional groups to obtain a deeper understanding of the mechanisms of formation of polymer:fullerene BHJ films and their effects on the photovoltaic properties.

ASSOCIATED CONTENT

S Supporting Information

Experimental details for polymer synthesis and characterization, solar cell device fabrication and measurements, and GIXD and surface energy measurements. This material is available free of charge via the Internet at <http://pubs.acs.org>.

AUTHOR INFORMATION

Corresponding Author

*(H.J.S.) E-mail: hjsong@kist.re.kr.

Author Contributions

○These authors equally contributed to this work

Notes

The authors declare no competing financial interest.

ACKNOWLEDGMENTS

This work was supported by the Global Frontier R&D Program on Center for Multiscale Energy System funded by the National Research Foundation under the Ministry of Science, and Korea Institute of Science and Technology (KIST) for Project No. 2E25390 and No. 2V04000. K.K. expresses thanks for financial support from NRF Fund No. 2009-0093817.

REFERENCES

- Dou, L.; You, J.; Hong, Z.; Xu, Z.; Li, G.; Street, R. A.; Yang, Y. *Adv. Mater.* **2013**, *25*, 6642–6671.
- Dang, M. T.; Hirsch, L.; Wantz, G.; Wuest, J. D. *Chem. Rev.* **2013**, *113*, 3734–3765.
- Krebs, F. C.; Espinosa, N.; Hösel, M.; Søndergaard, R. R.; Jørgensen, M. *Adv. Mater.* **2014**, *26*, 29–39.
- Huang, Y.; Kramer, E. J.; Heeger, A. J.; Bazan, G. C. *Chem. Rev.* **2014**, *114*, 7006–7043.
- Hains, A. W.; Liang, Z.; Woodhouse, M. A.; Gregg, B. A. *Chem. Rev.* **2010**, *110*, 6689–6735.
- Gordon, J.; Hedley, G. J.; Ward, A. J.; Alekseev, A.; Howells, C. T.; Martins, E. R.; Serrano, L. A.; Cooke, G.; Ruseckas, A.; Samuel, I. D. W. *Nat. Commun.* **2013**, *4*, 2867.

- (7) Lee, J. K.; Ma, W. L.; Brabec, C. J.; Yuen, J.; Moon, J. S.; Kim, J. Y.; Lee, K.; Bazan, G. C.; Heeger, A. J. *J. Am. Chem. Soc.* **2008**, *130*, 3619–3623.
- (8) Li, G.; Zhu, R.; Yang, Y. *Nat. Photonics* **2012**, *6*, 153–161.
- (9) Lee, J. K.; Ma, W. L.; Brabec, C. J.; Yuen, J.; Moon, J. S.; Kim, J. Y.; Lee, K.; Bazan, G. C.; Heeger, A. J. *J. Am. Chem. Soc.* **2008**, *130*, 3619–3623.
- (10) Zhou, H.; Zhang, Y.; Seifert, J.; Collins, S. D.; Luo, C.; Bazan, G. C.; Nguyen, T.-Q.; Heeger, A. J. *Adv. Mater.* **2013**, *25*, 1646–1652.
- (11) Chang, S.-Y.; Liao, H.-C.; Shao, Y.-T.; Sung, Y.-M.; Hsu, S.-H.; Ho, C.-C.; Su, W.-F.; Chen, Y.-F. *J. Mater. Chem. A* **2013**, *1*, 2447–2452.
- (12) Yang, X.; Loos, J.; Veenstra, S. C.; Verhees, W. J. H.; Wienk, M. M.; Kroon, J. M.; Michels, M. A. J.; Janssen, R. A. J. *Nano Lett.* **2005**, *5*, 579–583.
- (13) Perez, M. D.; Borek, C.; Forrest, S. R.; Thompson, M. E. *J. Am. Chem. Soc.* **2009**, *131*, 9281–9286.
- (14) Credgington, D.; Durrant, J. R. *J. Phys. Chem. Lett.* **2012**, *3*, 1465–1478.
- (15) Koen Vandewal, K.; Tvingstedt, K.; Gadisa, A.; Inganäs, O.; Manca, J. V. *Nat. Mater.* **2009**, *8*, 904–909.
- (16) Brabec, C. J.; Heeney, M.; McCulloch, I.; Nelson, J. *Chem. Soc. Rev.* **2011**, *40*, 1185–1199.
- (17) Liu, F.; Zhao, W.; Tumbleston, J. R.; Wang, C.; Gu, Y.; Wang, D.; Briseno, A. L.; Ade, H.; Russell, T. P. *Adv. Energy Mater.* **2014**, *4*, 1301377.
- (18) Cheng, Y.-J.; Yang, S.-H.; Hsu, C.-S. *Chem. Rev.* **2009**, *109*, 5868–5923.
- (19) Thompson, B. C.; Kim, B. J.; Kavulak, D. F.; Sivula, K.; Mauldin, C.; Fréchet, J. M. *Macromolecules* **2007**, *40*, 7425–7428.
- (20) Zhou, H.; Yang, L.; Xiao, S.; Liu, S.; You, W. *Macromolecules* **2009**, *43*, 811–820.
- (21) Liang, Y.; Feng, D.; Wu, Y.; Tsai, S.-T.; Li, G.; Ray, C.; Yu, L. J. *Am. Chem. Soc.* **2009**, *131*, 7792–7799.
- (22) Kim, H.; Lee, B. H.; Lee, K. C.; Kim, G.; Yu, J. Y.; Kim, N.; Lee, S. H.; Lee, K. *Adv. Energy Mater.* **2013**, *3*, 1575–1580.
- (23) Wang, E.; Bergqvist, J.; Vandewal, K.; Ma, Z.; Hou, L.; Lundin, A.; Himmelberger, S.; Salleo, A.; Müller, C.; Inganäs, O.; Zhang, F.; Andersson, M. R. *Adv. Energy Mater.* **2013**, *3*, 806–814.
- (24) Meager, I.; Ashraf, R. S.; Mollinger, S.; Schroeder, B. C.; Bronstein, H.; Beatrup, D.; Vezie, M. S.; Kirchartz, T.; Salleo, A.; Nelson, J.; McCulloch, I. *J. Am. Chem. Soc.* **2013**, *135*, 11537–11540.
- (25) Miller, N. C.; Sweetnam, S.; Hoke, E. T.; Gysel, R.; Miller, C. E.; Bartelt, J. A.; Xie, X.; Toney, M. F.; McGehee, M. D. *Nano Lett.* **2012**, *12*, 1566–1570.
- (26) Mayer, A.; Toney, M. F.; Scully, S. R.; Rivnay, J.; Brabec, C. J.; Scharber, M.; Koppe, M.; Heeney, M.; McCulloch, I.; McGehee, M. D. *Adv. Funct. Mater.* **2009**, *19*, 1173–1179.
- (27) Kim, J. S.; Lee, Y.; Lee, J. H.; Park, J. H.; Kim, J. K.; Cho, K. *Adv. Mater.* **2010**, *22*, 1355–1360.
- (28) Walker, B.; Tamayo, A.; Duong, D. T.; Dang, X.-D.; Kim, C.; Granstrom, J.; Nguyen, T.-Q. *Adv. Energy Mater.* **2011**, *1*, 221.
- (29) Barton, A. F. M. *Handbook of Solubility Parameters*; CRC Press: Boca Raton, FL, 1983; pp 153–157.
- (30) Machui, F.; Abbott, S.; Waller, D.; Koppe, M.; Brabec, C. J. *J. Polym. Sci., Part B* **2012**, *50*, 1405–1413.
- (31) Hansen, C. M. *Hansen Solubility Parameters: a User's Handbook*, 2nd ed.; CRC Press: Boca Raton, FL, 2007; Chapter 1.
- (32) He, Z.; Zhong, C.; Su, S.; Xu, M.; Wu, H.; Cao, Y. *Nat. Photonics* **2012**, *6*, 591–595.
- (33) Liang, Y.; Xu, Z.; Xia, J.; Tsai, S.-T.; Wu, Y.; Li, G.; Ray, C.; Yu, L. *Adv. Mater.* **2010**, *22*, E135–E138.
- (34) Liang, Y.; Wu, Y.; Feng, D.; Tsai, S.-T.; Son, H. J.; Yu, L. *J. Am. Chem. Soc.* **2009**, *131*, 56–57.
- (35) Carsten, B.; He, F.; Son, H. J.; Xu, T.; Yu, L. *Chem. Rev.* **2011**, *111*, 1493–1528.
- (36) Bredas, J.-L. *Mater. Horiz.* **2014**, *1*, 17–19.
- (37) Thompson, B. C.; Fréchet, J. M. *Angew. Chem., Int. Ed.* **2008**, *47*, 58–77.
- (38) Szarko, J. M.; Guo, J.; Liang, Y.; Lee, B.; Rolczynski, B. S.; Strzalka, J.; Xu, T.; Loser, S.; Marks, T. J.; Yu, L.; Chen, L. X. *Adv. Mater.* **2010**, *22*, 5468–5472.
- (39) Chen, W.; Xu, T.; He, F.; Wang, W.; Wang, C. S.; Strzalka, J.; Liu, Y.; Wen, J.; Miller, D. J.; Chen, J.; Hong, K.; Yu, L.; Darling, S. B. *Nano Lett.* **2011**, *11*, 3707–3713.
- (40) Hunter, C. A.; Sanders, J. K. *J. Am. Chem. Soc.* **1990**, *112*, 5525–5534.
- (41) Woo, C. H.; Thompson, B. C.; Kim, B. J.; Toney, M. F.; Frechet, J. M. *J. Am. Chem. Soc.* **2008**, *130*, 16324–16329.
- (42) Kawase, T.; Kurata, H. *Chem. Rev.* **2006**, *106*, 5250–5273.
- (43) Ruoff, R.; Tse, D. S.; Malhotra, R.; Lorents, D. C. *J. Phys. Chem.* **1993**, *97*, 3379–3383.
- (44) Israelachvili, J. N. *Intermolecular & Surface Forces*, 2nd ed.; Academic Press: San Diego, CA, 2009; Chapter 9.
- (45) Grimme, S.; Ehrlich, S.; Goerigk, L. *J. Comput. Chem.* **2011**, *32*, 1456–1465.
- (46) Pivrikas, A.; Juška, G.; Mozer, A. J.; Scharber, M.; Arlauskas, K.; Sariciftci, N. S.; Stubb, H.; Österbacka, R. *Phys. Rev. Lett.* **2005**, *94*, 176806.
- (47) Pivrikas, A.; Sariciftci, N.; Juška, G.; Österbacka, R. *Prog. Photovolt: Res. Appl.* **2007**, *15*, 677–696.
- (48) Veldman, D.; Meskers, S. C. J.; Janssen, R. A. J. *Adv. Funct. Mater.* **2009**, *19*, 1939–1948.
- (49) Moulé, A.; Meerholz, K. *Appl. Phys. B: Laser Opt.* **2008**, *92*, 209–218.
- (50) Koster, L. J. A.; Mihailescu, V. D.; Xie, H.; Blom, P. W. M. *Appl. Phys. Lett.* **2005**, *87*, 203502.
- (51) Cowan, S. R.; Roy, A.; Heeger, A. J. *Phys. Rev. B* **2010**, *82*, 245207.
- (52) He, Y.; Shao, M.; Xiao, K.; Smith, S. C.; Hong, K. *Sol. Energy Mater. Sol. Cells* **2013**, *118*, 171–178.
- (53) Drees, M.; Hoppe, H.; Winder, C.; Neugebauer, H.; Sariciftci, N. S.; Schwinger, W.; Schaffler, F.; Topf, C.; Scharber, M. C.; Zhu, Z.; Gaudiana, R. *J. Mater. Chem.* **2005**, *15*, 5158.
- (54) Theander, M.; Yartsev, A.; Zigmantas, D.; Sundström, V.; Mammo, W.; Andersson, M. R.; Inganäs, O. *Phys. Rev. B* **2000**, *61*, 12957.
- (55) Zhang, F.; Perzon, E.; Wang, X.; Mammo, W.; Andersson, M. R.; Inganäs, O. *Adv. Funct. Mater.* **2005**, *15*, 745–75.